

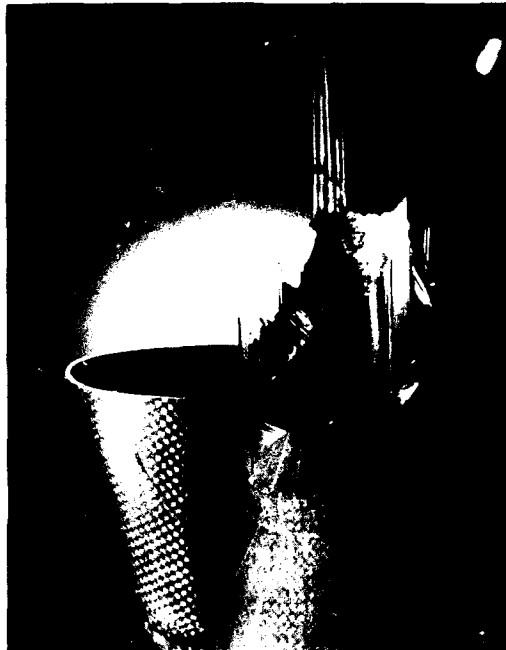
AD-A250 518



0597

CENTER FOR MECHANICS OF COMPOSITES

DTIC
MAY 2 0 1992



CMC REPORT NO. 6730-15

The Mechanics of Fractal Damage

Ted L. Anderson
Sun Yongqi

March 30, 1992

TEXAS ENGINEERING EXPERIMENT STATION
THE TEXAS A&M UNIVERSITY SYSTEM

92-12944



REPORT DOCUMENTATION PAGE

Form Approved
OMB No. 0704-0188

This report is the property of the Air Force Office of Scientific Research. It is loaned to you for your use only. It is not to be distributed outside your organization. It is to be returned to the Air Force Office of Scientific Research, 3150 Jefferson Davis Highway, Suite 1204, Arlington, VA 22202-4302, and to the Office of Management and Budget, Paperwork Reduction Project (0704-0188), Washington, DC 20503.

1. AGENCY USE ONLY (Leave blank)	2. REPORT DATE 30 March 1992	3. REPORT TYPE AND DATES COVERED Final Report 30 Sept 90 - Jan 92
----------------------------------	---------------------------------	--

4. TITLE AND SUBTITLE The Mechanics of Fractal Damage (u)	5. FUNDING NUMBERS G AFOSR-90-0373
---	---

6. AUTHOR(S) Ted L. Anderson Sun Yongqi	
---	--

7. PERFORMING ORGANIZATION NAME(S) AND ADDRESS(ES) Department of Mechanical Engineering Texas A&M University College Station, Texas 77843	8. PERFORMING ORGANIZATION REPORT NUMBER CMC-6730-15
--	---

9. SPONSORING / MONITORING AGENCY NAME(S) AND ADDRESS(ES) Air Force Office of Scientific Research Aerospace Sciences Division Bolling AFB, DC 20332	10. SPONSORING / MONITORING AGENCY REPORT NUMBER
--	--

11. SUPPLEMENTARY NOTES

12a. DISTRIBUTION AVAILABILITY STATEMENT	12b. DISTRIBUTION CODE
--	------------------------

13. ABSTRACT (Maximum 200 words)

This report describes a preliminary investigation of the applicability of fractal geometry to damage modeling. Microstructural heterogeneity, both the size distribution and spatial distribution of microstructural features, can be modeled simply and compactly with a fractal dimension. The ultimate goal of this research is the development of an alternative to continuum damage and micromechanics models. The scaling nature of fractal geometry may aid the development of models that connect microscale damage with global mechanical response.

An assumed fractal size distribution of microcracks in a brittle solid was used to derive the Weibull distribution for strength, and a relationship between the Weibull shape parameter and the fractal dimension of the flaw distribution was obtained. Published data on the strength of glass fibers were consistent with a fractal flaw distribution. Stable damage evolution in tougher materials with fractal microstructures was also considered.

Although preliminary results are promising, further work is necessary to develop the concepts of fractal damage more fully.

14. SUBJECT TERMS Damage Mechanics, Micromechanics, Composite Materials, Fractal Geometry.	15. NUMBER OF PAGES 30
	16. PRICE CODE

17. SECURITY CLASSIFICATION OF REPORT Unclassified	18. SECURITY CLASSIFICATION OF THIS PAGE Unclassified	19. SECURITY CLASSIFICATION OF ABSTRACT Unclassified	20. LIMITATION OF ABSTRACT UL
---	--	---	----------------------------------

THE MECHANICS OF FRACTAL DAMAGE

Final Report

Air Force Office of Scientific Research
Division of Aerospace Sciences
United States Air Force
Grant No. AFOSR-90-0373

Prepared by

Ted L. Anderson
Sun Yongqi

Department of Mechanical Engineering
Texas A&M University
College Station Texas 77843

CMC-6730-15

March 30, 1992.

SEARCHED
SERIALIZED
INDEXED
FILED
MAR 31 1992
AFOSR-90-0373
A-1

ABSTRACT

This report describes a preliminary investigation of the applicability of fractal geometry to damage modeling. Microstructural heterogeneity, both the size distribution and spatial distribution of microstructural features, can be modeled simply and compactly with a fractal dimension. The ultimate goal of this research is the development of an alternative to continuum damage micromechanics models. The scaling nature of fractal geometry may aid the development of models that connect microscale damage with global mechanical response.

An assumed fractal size distribution of microcracks in a brittle solid was used to derive the Weibull distribution for strength, and a relationship between the Weibull shape parameter and the fractal dimension of the flaw distribution was obtained. Published data on the strength of glass fibers were consistent with a fractal flaw distribution. Stable damage evolution in tougher materials was also considered. Recent work by Schapery on path-independent potentials combined with the fractal description of microscale damage shows promise as a framework for formulating damage models.

A limited amount of experimental validation of the fractal description of microstructure was obtained. Fractal clustering of second-phase particles in a polyvinyl chloride (PVC) sample, for example, led to a self-similar distribution of microvoids on the fracture surface. In certain other cases, however, microstructural features do not exhibit self-similar fractal characteristics. For example, damage zones that form during Mode II delamination of graphite-epoxy composites contain an array of regularly spaced microcracks that are all approximately the same size.

Although preliminary results are promising, further work is necessary to develop the concepts of fractal damage more fully.

CONTENTS

1.0 INTRODUCTION	1
2.0 A PRIMER ON FRACTALS.....	2
3.0 THE CONCEPT OF FRACTAL MICROSTRUCTURES	5
3.1 Fractal Size Distribution.....	5
3.2 Fractal Clustering.....	7
4.0 APPLICATIONS TO DAMAGE MODELING.....	7
4.1 Brittle Fracture.....	7
4.2 Stable Growth of Microcracks.....	9
4.3 Microcrack Toughening	12
4.4 Path-Independent Potentials.....	12
5.0 EXPERIMENTAL EVIDENCE FOR FRACTAL MATERIALS.....	17
5.1 Flaw Distribution in Glass	17
5.2 Clustering in Rubber-Toughened PVC.....	18
5.3 Mode II Delamination of Graphite/Epoxy Laminates.....	18
6.0 SUMMARY AND CONCLUSIONS.....	20
7.0 REFERENCES	21

1.0 INTRODUCTION

Most modern engineering materials contain microstructural heterogeneities such as fibers, whiskers, particulates, and second-phase particles. These constituents can greatly enhance mechanical and thermal properties. These new materials, however, were developed largely by trial and error, because our understanding of the relationships between processing, structure, and properties is incomplete at best. Although it is now possible to tailor the elastic and thermal properties of composite materials, the *nonlinear* mechanical response of a given material cannot be predicted in advance.

Many composites and multiphase materials experience microscale damage prior to ultimate failure. This subcritical damage often produces a toughening effect in the material. For example, two brittle ceramics can be combined to produce a relatively tough ceramic composite, because initial cracking in such materials dissipates energy without causing catastrophic failure [1].

A substantial number of researchers are studying damage development in advanced materials. Two basic approaches to this problem have emerged. *Continuum damage models* assume the material to be a homogeneous continuum, and treat damage development through internal state variables. Discrete phenomena such as fibers, particles, microcracks and voids are averaged through the material. *Micromechanics models*, however, consider events at the microscopic level, such as microcracking, fiber/matrix debonding, and void formation. These models usually analyze a unit cell, such as single fiber surrounded by matrix; an implicit assumption of such models is that the material as a whole consists of a periodic array of these unit cells.

Both types of damage model have advantages and disadvantages. Continuum models are computationally simpler, but they omit important microstructural information in their formulation. Such models are descriptive rather than predictive; numerous experiments are often required to specify adjustable parameters in these models. Micromechanics models provide information at the local level, but are computationally expensive, and the connection between these local models and global behavior requires a number of assumptions.

A unified model that simultaneously considers local damage and global response is not currently available. Modeling an entire structure with a mi-

micromechanics methodology would require hundreds or even thousands of unit cells, a level of complexity that is well beyond current computational capabilities. An approach that contains sufficient detail to model the problem adequately, yet is reasonably simple, could make a substantial contribution to this field.

Fractal geometry [2] is a relatively new branch of mathematics that is capable of describing complex and disordered phenomena simply and compactly. The scaling nature of fractals suggests a potential application as a "mesomechanics [3]" tool. That is, this discipline may provide a means to connect microstructural detail with macroscopic behavior without resorting to enormous computer models. A number of applications of fractal geometry to materials science have already been identified. The Materials Research Society has devoted several symposia to this topic [4-6].

This study represents a brief exploration of the possibilities for fractals in the areas of micromechanics and damage modeling. Although it is unlikely that fractal geometry will prove to be a panacea, the preliminary results described herein are sufficiently promising to encourage further study.

2.0 A PRIMER ON FRACTALS

The term "fractal" was coined by Mandelbrot [2] to describe a particular phenomena in nature; *fractal geometry* is the name he has given to the branch of mathematics that has developed in the past century to characterize these phenomena. In his 1982 book, Mandelbrot considers such diverse topics as the shape of clouds, the length of coastlines, the spatial distribution of celestial bodies, and Brownian motion. In each case, he shows that seemingly complex phenomena can be described simply and succinctly with a *fractal dimension*.

In Euclidean geometry, the dimensionality of shapes and objects is always an integer: lines and curves are one-dimensional, planes and surfaces are two-dimensional, and solid shapes are three-dimensional. Fractal objects, however, usually have a *fractional* dimension. Fractal curves, for example, typically have a dimensionality between 1 and 2, and the dimensionality of a fractal plane is between 2 and 3.

Consider a jagged coastline, such as the west coast of Britain (or, to take a more extreme example, consider the fiords of Norway). If one wanted to measure the length of this coastline, a reasonable first step might be to use a pair of dividers set to a known spacing and "step" the dividers along a map of the coastline. Such a measurement would not yield the "true" length; rather it would be based on an approximation of the coastline as a series of line segments. The length measurement would undoubtedly change if the setting on the dividers was adjusted. A man walking along this coastline could estimate its length by counting his steps and multiplying by the length of each stride. If he stayed as close as possible to the water's edge, he would take a much more meandering path than the dividers on the map, because the coast contains numerous inlets and other irregularities that are too small to be represented on a map. Consequently, he would walk a much greater distance than the length estimate from the map. Similarly, an ant walking along the water's edge would travel further than the man if both creatures covered the same segment of coastline.

Figure 1 shows coastline measurements for a number of locations throughout the world [2]. With the exception of the South African Coast, the measured coastline length increases with decreasing length of line segment, and the trends are linear on a log-log plot. This type of relationship is indicative of fractal curves, as discussed below. Note that when a Euclidean shape such as a circle is approximated by a series of line segments (i.e., a polygon), the measured perimeter converges to the true value as the length of the segments decrease. The measured length of the fractal coastlines do not converge, however.

For the curves in Fig. 1 that are linear, the measured length, L , can be represented by a power law:

$$L = L_0 \epsilon^{-m} = N \epsilon \quad (1)$$

where ϵ is the size of the line segment and N is the number of segments. Solving for N gives

$$N = L_0 \epsilon^{-(m+1)} = L_0 \epsilon^{-D} \quad (2)$$

The number of line segments required to approximate a Euclidean curve is inversely proportional to the segment length (ϵ); $m = 0$ and $D = 1$ in this case. Similarly, if a Euclidean surface were paved with square tiles with sides of length ϵ , the number of tiles required to cover the surface would be proportional to ϵ^{-2} . Thus D represents the dimensionality of the object. A fractal curve, such as the coastline of Britain, typically lies somewhere between a one-dimensional and two-dimensional object¹; D is the *fractal dimension* in this case.

An implicit assumption of fractal geometry is that the exponent D is independent of ϵ . Provided this assumption is approximately valid over several orders of magnitude, a fractal description of a natural phenomenon can be very useful.

It is possible to construct shapes for which the fractal description is rigorously correct. Figure 2 shows a Koch snowflake [2]. This shape is constructed through an infinite number of operations on a six-sided star, as Fig. 2 illustrates. *The perimeter of this object is infinite, but the area enclosed by the fractal curve is finite. Also, the derivatives are undefined at all points along the boundary.* The exact value of the fractal dimension of the Koch snowflake is $\log 4 / \log 3$. The Koch snowflake and similar constructions can be used to model natural phenomena such as coastlines, although the latter contains a degree of randomness that the idealizations do not consider.

A key feature of many fractals is that they are self-similar. Consider a segment of the boundary of the Koch snowflake in Fig. 2. If the curve were viewed at higher magnifications, its appearance would not change; *a self-similar fractal looks identical at all length scales.*

A number of investigators [7-10] have used fractal geometry to study fracture in engineering materials. In a brittle material, the fracture toughness (in terms of critical energy release rate, G_c) is two times the surface energy, γ_s , provided the fracture surface is smooth (i.e., Euclidean). If the fracture surface is fractal, however, the toughness depends on the scale of examination. At the atomic scale, $G_c = 2\gamma_s$, but the macroscopic toughness is higher because the effective area of a rough fracture surface is significantly larger than the projected area. If the area is measured by paving the surface with squares, as dis-

¹A fractal curve that lies in a plane can have a fractal dimension as high as 2, in which case the curve completely fills the plane.

cussed above, the measured area is proportional to ϵ^{2-D} . The macroscopic toughness can be estimated from the ratio of the projected area of the sample (L^2) to the measured area at the atomic scale:

$$G_c \approx 2 \gamma_s \left(\frac{L}{a_0} \right)^{D-2} \quad (3)$$

where L is a characteristic sample dimension and a_0 is the atomic size. Equation (3) indicates that toughness increases with increasing D ; the enhanced toughness is a result of the additional surface area created during fracture. Although there is often a connection between fractal dimension and toughness in brittle materials, such a relationship is usually not observed in more ductile materials. In ductile metals, for example, most of the fracture energy is dissipated through dislocation motion; there is not necessarily a direct relationship between the fracture work and the amount of surface area created.

3.0 THE CONCEPT OF FRACTAL MICROSTRUCTURES

Fractal geometry not only characterizes many non-Euclidean shapes such as coastlines, mountain ranges, and fracture surfaces, the methodology can also describe various types of disorder and heterogeneity. In this study, we considered two types of fractal description for microstructural heterogeneity. Most of the focus was on *fractal size distribution*; in real materials, entities such as microcracks and second-phase particles are seldom of a uniform size. In addition, we briefly addressed disordered *spatial distribution* of microstructural features.

3.1 Fractal Size Distribution

Consider a material of volume V which contains microcracks of various sizes. If we assume that these cracks are distributed in size as a scaling fractal, the cumulative microcrack density, ρ , will follow a hyperbolic distribution:

$$\rho(a_c) = \frac{Nr(a > a_c)}{V} = \lambda a_c^{-D} \quad (4)$$

where a is a characteristic crack dimension, a_c is a reference crack size, λ is a constant, and D is the fractal dimension. The notation $Nr()$ refers to the number of microcracks for which the statement in parentheses is satisfied; in this case, the number of microcracks greater than a given size.

The incremental microcrack density can be approximated by

$$\Delta\rho(a_c) = \frac{Nr(a_c < a < a_c + \Delta a)}{V} = D\lambda a_c^{-(D+1)}\Delta a \quad (5)$$

provided $\Delta a \ll a_c$. Thus both ρ and $\Delta\rho$ follow power-law distributions. Although there appears to be nothing particularly striking about a power-law distribution for microcrack size, the exponent D has a particular physical significance, as explained below.

In real materials there is an upper limit on the microcrack size. Re-integrating Eq. (2) with an upper threshold crack size, a_u , gives:

$$\rho(a_c, a_u) = \lambda(a_c^{-D} - a_u^{-D}) \quad \text{for } a_c < a_u \quad (6)$$

This relationship obviously reduces to Eq. (4) when $a_c \ll a_u$.

If Eq. (6) describes the distribution of an array of penny shaped cracks, where a is the crack radius, the cumulative surface area in a unit volume is given by

$$S = \frac{\pi D \lambda}{2-D} (a_u^{2-D} - a_c^{2-D}) \quad (7)$$

When $a_c \ll a_u$ and $D \neq 2$, one of the terms in parentheses dominates, depending on the value of D . If $D > 2$, the cumulative area is asymptotic to $a_c = 0$; thus the microcracks form a fractal surface. When $D < 2$, the cumulative area is finite and is controlled primarily by the largest cracks. (Note that the upper limit, a_u , is necessary in this latter case; conventional fractal theory implies that a_u is infinite, which would make the cumulative area zero if $D < 2$.)

If a stress were applied to the material such that the crack faces moved apart, the resulting volume increase for a particular crack would be proportional to a^3 . Thus it can be shown that D must be less than three in order for the total sample volume to remain finite.

3.2 Fractal Clustering

The spatial distribution of microcracks or other microstructural features may also be amenable to a fractal description. Figure 3 shows an idealized (2-D) example of fractal clustering, where particles form clusters, which form larger clusters, and so on. Note the self-similarity of the structure, such that its appearance is identical at all scales. For this example, $D = 1$.

Of course real microstructures exhibit some degree of randomness, and thus do not form regular patterns as in Fig. 3. However, there is evidence that certain materials exhibit some degree of fractal clustering, as discussed below. This self-similar structure may greatly simplify micromechanical modeling of such materials.

4.0 APPLICATIONS TO DAMAGE MODELING

4.1 Brittle Fracture

In brittle materials, a flaw becomes unstable when the Griffith energy criterion is satisfied. For a penny shaped crack, the critical stress (applied normal to the crack plane) is given by

$$\sigma_f = \sqrt{\frac{\pi E w_f}{2 a_c}} \quad (8)$$

where σ_f is the fracture stress, E is Young's modulus, a_c is the critical crack radius, and w_f is the fracture work per unit area. For ideally brittle solids, w_f is the surface energy, γ_s . For quasi-brittle materials, such as BCC metals on the lower shelf of toughness, w_f includes a plastic work component.

Brittle fracture is, by nature, a weakest link phenomenon. Only one flaw need satisfy the Griffith criterion to cause failure. Thus the largest or most

favorably oriented flaw in a material dictates the fracture strength. If a specimen of volume V contains ρ critical flaws per unit volume, where ρ is small and V is large, the failure probability is given by

$$F = 1 - \exp(-\rho V) \quad (9)$$

Equation (9) is a special case of the Poisson distribution; F is equal to the probability of sampling at least one critical flaw in V .

Consider a uniaxial tensile specimen of volume V with a fractal distribution of penny shaped microcracks oriented perpendicular to the stress axis². Combining Eqs. (4), (8) and (9) gives

$$F = 1 - \exp\left(-V\left(\frac{\sigma_f}{\Theta}\right)^{2D}\right) \quad (10)$$

where

$$\Theta = \sqrt{\frac{2\lambda^{1/D}}{\pi E w_f}}$$

Equation (10) has the form of a Weibull distribution on fracture stress. The Weibull shape parameter (or slope) is $2D$. Weibull [11] originally suggested this distribution for characterizing the strength of brittle materials because it seemed to fit experimental data. Invoking fractal geometry provides a physical basis for the Weibull distribution. There is a direct correspondence between Weibull slope and the fractal dimension of the flaw distribution. When an upper cut-off on crack size is imposed (Eq. 6) the distribution becomes

$$F = 1 - \exp\left(-V\left(\left(\frac{\sigma_f}{\Theta}\right)^{2D} - \left(\frac{\sigma_u}{\Theta}\right)^{2D}\right)\right) \quad (11)$$

²Allowing for randomly oriented microcracks would not change the results. Given a crack of radius a whose normal forms an angle ϕ with the stress axis, it is possible to define an effective crack radius $a^* = a^*(a, \phi)$ which satisfies Eq. [8] at fracture. If the distribution of a is hyperbolic, a^* should also be hyperbolic.

where σ_u is the threshold fracture stress corresponding to the maximum crack size, a_u . Equation (11) is a *truncated* Weibull distribution.

According to Eqs. (10) and (11), the Weibull slope cannot be greater than 6 if the flaw distribution is fractal. However, the published literature contains numerous fracture strength data with Weibull slopes in excess of 6. For example, Wiederhorn and Fuller [12] report Weibull slopes of 7.0 for ordinary glass and 9.8 for an Al_2O_3 ceramic. Wagner, et al. [13] measured slopes ranging from 4.1 to 10.5 for various aramid filaments.

The threshold stress, σ_u , offers a potential explanation for the discrepancy between the expected range of Weibull slopes and experimental values. The authors mentioned above used a two parameter Weibull formulation (Eq. 10) which may have led to artificially high Weibull slopes. Sample calculations with Eq. (11) illustrate this point. Figure 4 is a plot of Eq. (11) (on a two parameter Weibull graph) assuming that $\sigma_u = 1000$ MPa, $2D = 4.0$, and $\Theta = 8400$ MPa mm^{0.75}. Distributions are plotted for sample volumes ranging over several orders of magnitude. The curve for the smallest volume is nearly linear with a slope of 4.0. As volume increases, the fracture stress tends to decrease, and the apparent Weibull slope (on the two parameter graph) increases. As the samples become very large, the probability of sampling a microcrack with radius close to a_u in each specimen approaches 1, and the apparent Weibull slope approaches infinity.

A three-parameter distribution of the form of Eq. (11) may be more realistic than the two parameter formulation. It would be interesting to apply Eq. (11) to the data in [12] and [13] to see if D is less than 3 in each case. Unfortunately the authors of these articles did not report individual σ_f values.

4.2 Stable Growth of Microcracks

At initiation of crack growth, the applied energy release rate, G , equals the material's resistance to crack extension, R . For brittle materials, $R = 2w_f = \text{constant}$; fracture tends to be unstable because an increase in G cannot be matched by the material resistance. For stable crack advance, the following condition must be met:

$$dG(\sigma, a) = dR(a) \quad (12)$$

Crack propagation will be unstable if $dG > dR$. Stable crack extension usually requires R to increase with crack growth. However, this need not be the case because there are certain configurations for which G decreases with crack extension. Equation (12) can be written as

$$\frac{\partial G}{\partial \sigma} d\sigma + \frac{\partial G}{\partial a} da = \frac{dR}{da} da \quad (13)$$

For a penny shaped crack with stress applied perpendicular to the crack plane,

$$G = \frac{4 \sigma^2 a}{\pi E} \quad (14)$$

Substituting Eq. (13) into Eq. (14) and rearranging gives

$$\frac{da}{a} = \frac{8 \sigma d\sigma}{\pi E} \left(\frac{dR}{da} - \frac{4 \sigma^2}{\pi E} \right)^{-1} \quad (15)$$

If a material contains a distribution of penny shaped cracks and dR/da is the same for all crack sizes at a given stress level, da/a is also constant for all a . That is, the damage growth is self similar. In the example which follows, self similar crack growth is assumed.

Consider a uniaxial tensile specimen with cross sectional area A_s . Assume that the material contains a fractal distribution of microcracks (Eq. 6) which are oriented perpendicular to the stress axis. For this example, it is assumed that the microcracks do not interact with the specimen boundaries or each other³. Crack growth will result in a loss in stiffness in the specimen. The definition of G based on elastic compliance can be invoked to estimate the stiffness loss:

$$G = \frac{P^2}{2} \frac{\partial C}{\partial A} \quad (16)$$

³Crack interaction would have the effect of making each crack behave as if it were somewhat larger or smaller. These effects could be modeling by assuming a fractal distribution of the effective crack size.

where P is the applied force, A is the crack area and C is the elastic compliance (= displacement/force). For a single penny shaped crack in the tensile specimen, the increase in compliance due to a crack extension da is given by

$$dC = \frac{16 a^2 da}{E A_s^2} \quad (17)$$

The specimen in the present example contains a distribution of microcracks, each of which will contribute to the compliance increase as it grows. Thus the total compliance change is determined by summing the contributions of all flaws:

$$dC = -V \int_0^{a_u} dC(a) \frac{\partial \rho}{\partial a} da \quad (18)$$

Note that this integral is taken over a constant state of damage. The integrand is obtained from Eqs. (6), (15) and (17). This integral can then be solved directly by assuming dR/da does not depend on crack size. Furthermore, one can obtain an expression for the change in effective modulus, E^* , by noting that $C = V/(E^* A_s)$. That is,

$$dE^* = - \frac{128 \sigma D \rho_u a_u^3}{\pi (3-D)} \left(\frac{E^*}{E} \right)^2 \left(\frac{dR}{da} - \frac{4 \sigma^2}{\pi E} \right)^{-1} d\sigma \quad (19)$$

where $\rho_u = \lambda a_u^{-D}$. Both λ and a_u change with crack growth but ρ_u is constant. In addition, the assumption of self similar damage (i.e., da/a is independent of crack size at a given stress) implies that D is also constant. Note that the integral in Eq. (18) was solved by assuming $D < 3$; a fractal dimension greater than three is physically inadmissible in this case because such a value would imply that modulus increases without bound when a finite stress is applied.

Figure 5 illustrates the stress-strain behavior of a material modeled by Eq. (19). A change in stress, $d\sigma$, results in a decrease in effective modulus, dE^* . The entire uniaxial constitutive behavior of this material is obtained by integrating the above equation from the initial damage state to final instability.

Note that the present analysis does not consider dilatational effects due to the open cracks. It is assumed that the material would return to zero stress and strain if unloaded.

The above example is obviously an oversimplification of real material behavior. One would normally expect the slope of the material resistance curve (dR/da) to depend on crack size. In addition, real microcracks would not be perfectly flat and penny shaped as was assumed. In fact there may be a separate fractal dimension associated with the microcrack shape. Finally, the above derivation did not consider a more general three dimensional state of stress.

4.3 Microcrack Toughening

Microcrack formation dissipates energy, and thus produces a toughening effect, provided a microcrack does not become unstable and lead to complete failure. Consider a macroscopic crack, with current length c , propagating in a solid. Suppose that this macroscopic crack produces a process zone of microcracks on either side of the crack plane, as Fig. 6 illustrates. Assuming a unit out-of-plane dimension for the sample, the global energy release rate for this crack corresponds to the work dissipated in the volume $2h dc$, divided by dc . If the flaw distribution is fractal (with an upper cut-off) and the work dissipated by each microcrack is $2\pi \gamma_s a^2$, the global toughness is given by

$$G_c = \frac{4\pi h \gamma_s D \lambda}{2-D} (a_u^{2-D} - a_c^{2-D}) \quad (20)$$

If $D > 2$, the smallest microcracks would provide the largest contribution to fracture work, while the larger flaws would dominate if $D < 2$.

Equation (20) does not include the dilatational contribution to fracture work. Dilatational work would scale with the specific volume change, $\Delta V/V$, which is proportional to a_u^{3-D} , where $D < 3$.

4.4 Path-Independent Potentials

The damage models derived in previous sections are relatively simple. The analysis of effective modulus, for example, assumed uniaxial deformation

and non-interacting microcracks. Recent work by Schapery [14], which is described below, provides a mathematical framework for more detailed damage models for fractal materials. He showed that certain materials that sustain irreversible damage exhibit limited path independence and can be described with a potential function.

Consider a body that is subject to the generalized loads Q_j and generalized displacements q_j ($j = 1, 2, \dots, J$), where Q_j and q_j may correspond to stress and strain, load and displacement, moment and curvature, etc. The total work required to deform the body to q_j from an initially unloaded state can be expressed as follows:

$$W_T = W + W_S \quad (21)$$

where W_T is the total work, W is the strain energy, and W_S is the work dissipated during structural change. Equation (21) and the relationships that follow can be applied a global scale or to an infinitesimal point, provided derivatives are continuous throughout the body⁴. Let us assume that $W = W(q_j, S_m)$, where S_m ($m = 1, 2, \dots, M$) are (as yet unspecified) structure parameters, and that W exhibits the properties of an elastic potential:

$$Q_j = \frac{\partial W}{\partial q_j} \quad (22)$$

The total work, in terms of generalized forces and displacements, is given by

$$W_T = \int Q_j dq_j \quad (23)$$

Unless otherwise noted, the summation convention on repeated indices is followed throughout this report. The difference between total work and strain energy is that W_T is the work done on the body during the actual deformation process, while W is the work done when all S_m are held constant.

⁴Microcracks, voids and similar features are treated as boundaries in the body, in contrast to continuum damage models that average the effects of microstructural heterogeneity through the body.

The relationship between total work and strain energy can be derived by considering an infinitesimal change in W :

$$dW = \frac{\partial W}{\partial q_j} dq_j + \frac{\partial W}{\partial S_m} dS_m = Q_j dq_j - G_m dS_m \quad (24)$$

where G_m are the thermodynamic forces, defined as

$$G_m \equiv -\frac{\partial W}{\partial S_m} \quad (25)$$

Comparing Eqs. (23) and (24) leads to

$$W_T = W + \int G_m dS_m \quad (26)$$

Thus,

$$W_S = \int G_m dS_m \quad (27)$$

If it is assumed that W_S is a state function of the structure parameters, that is $W_S = W_S(S_m)$, the following is true when $\dot{S}_m \neq 0$:

$$G_m = \frac{\partial W_S}{\partial S_m}$$

or

$$G_m = R_m \quad (28)$$

where R_m are material resistance parameters. Equation (28) describes stable damage evolution. The thermodynamic driving force, G_m , is the energy *available* for structural changes, while R_m is the energy *required* for these changes. Thus Eq. (28) is a more general statement of the energy release rate-material resistance relationship of fracture mechanics (Eq. 12).

Suppose that during deformation, N structure parameters undergo change ($1 \leq N \leq M$), and the other $(M-N)$ parameters remain constant. Let us

now evaluate the variation in total work with respect to changes in S_n ($n = 1, 2, \dots, N$):

$$\frac{\partial W_T}{\partial S_n} = \frac{\partial W}{\partial S_n} + \frac{\partial W_S}{\partial S_n} = 0 \quad (29)$$

Thus total work is stationary with respect to changes in S_n . Schapery [14] argued that total work follows a minimum path, provided the body is taken through stable states. Consequently, a disturbance in the structure parameters, S_n , from their equilibrium values requires *positive* work. Conversely, it is possible to derive the S_n as functions only of q_j by minimizing the work. Thus $S_n = S_n(q_j)$ when Eq. (28) is satisfied, which implies $W_T = W_T(q_j)$. Therefore,

$$Q_j = \frac{\partial W_T}{\partial q_j} \quad (30)$$

That is, W_T displays the properties of an elastic potential. The total work is path independent for the $q_j(t)$ histories that produce changes in the same set of structure parameters, S_n .

The structure parameters can be defined in a variety of ways depending on the problem under consideration. Unlike most continuum damage models, however, where the internal state variables are essentially fitting parameters, the S_m can have a physical interpretation. In a macroscopic crack growth problem, for example, M can be set equal to 1, and S can denote the crack area. In this case, Eq. (28) reduces to the well-known result from fracture mechanics; i.e., $\mathcal{G} = R$ for stable crack growth. The material resistance may be a constant (such as in brittle materials where $R = 2\gamma_s$), or R can be a function of S .

Let us return to the problem of a body containing a fractal distribution of microcracks (Sections 4.1 to 4.3). Let S_m be the areas of individual penny-shaped cracks in the solid: $S_m = \pi a_m^2$. Assume that the microcracks grow according to a power law function of crack area:

$$\begin{aligned} R_m &= \alpha (\Delta S_m)^\beta \\ &= \alpha \pi (a_m^2 - a_{m(0)}^2) \end{aligned} \quad (31)$$

where α and β are material constants and $a_{m(0)}$ are the initial crack radii. The work dissipated in growing the microcracks from an initial state is given by

$$W_S = \int_{S_{m(0)}}^{S_m} \alpha (S_m - S_{m(0)})^\beta dS_m \quad (32)$$

The summation convention applies to S_m ; the contributions from each microcrack must be summed to obtain the total W_S . For the remainder of this derivation, we will drop the index notation and assume the crack size distribution is continuous. The energy dissipated by a single microcrack of (current) radius a is given by

$$w_s(\Delta a) = \frac{\alpha \pi (a^2 - a_{(0)}^2)^{\beta+1}}{\beta + 1} \quad (33)$$

If the initial flaw distribution is fractal (Eq. 5), the total work dissipated by cracks ranging in size from a_c to a_u is as follows:

$$\begin{aligned} W_S &= \int_{a_{c(0)}}^{a_{u(0)}} w_s(\Delta a) \frac{\partial \rho}{\partial a_{(0)}} da_{(0)} \\ &= \int_{a_{c(0)}}^{a_{u(0)}} \frac{\alpha \pi (\Phi^2 - 1)^{\beta+1} a_{(0)}^{(2\beta-D+1)}}{\beta + 1} da_{(0)} \end{aligned} \quad (34)$$

where $\Phi = (a + a_{(0)})/a_{(0)}$. If we assume, as a first approximation, that the damage growth is self-similar (i.e., Φ does not depend on $a_{(0)}$), Eq. (34) has a closed-form solution:

$$W_S = \frac{\alpha \pi (\Phi^2 - 1)^{\beta+1} (a_{u(0)}^{(2\beta-D+2)} - a_{c(0)}^{(2\beta-D+2)})}{(\beta + 1)(2\beta - D + 2)} \quad (35)$$

The assumption of self-similar damage is not strictly valid in this case, however. The relative damage growth, Φ , depends on flaw size in accordance to the assumed growth law (Eq. 31).

5.0 EXPERIMENTAL EVIDENCE FOR FRACTAL MATERIALS

The preceding analyses would ultimately be of little practical value unless examples of fractal microstructures could be found in nature. Although materials do not always exhibit the fractal properties discussed in Sections 3 and 4, there are cases where the fractal model fits quite well, as discussed below.

5.1 Flaw Distribution in Glass

Griffith, in his classic 1920 paper [15], reported data that are well suited to a test of the fractal model of flaw size distribution. He measured the strength of glass fibers of various sizes, and showed that the strength increased with decreasing sample volume, which is consistent with a weakest-link model for brittle fracture.

If we assume that the strength of a given fiber was controlled by the largest flaw in the sample, we can estimate the density (number/volume) of the critical flaw from the reciprocal of the sample volume. From Eq. (8), we know that the critical flaw size is proportional to σ_f^{-2} . Thus a plot of reciprocal volume versus strength⁻² should yield a straight line if the flaw size distribution in the material is fractal.

Figure 7 is a plot of flaw density ($1/V$) versus relative flaw size (σ_f^{-2}).⁵ The plot is linear over several decades, and the estimated fractal dimension is 1.34. As the sample volume becomes large, the curve deviates from the linear trend, as the critical flaw size reaches an upper limit. Thus Fig. 7 is consistent with Eq. (6).

⁵More quantitative estimates of flaw size can be inferred by substituting the appropriate modulus and surface energy into Eq. (8) and solving for a_c . However, we were only interested in the slope of the ρ versus a_c graph in this case.

Anderegg [16] performed a similar set of experiments on glass, but with a more limited range of sample volumes. The flaw density versus size graph is shown in Fig. 8. The trend is similar to Fig. 7, but $D = 2.46$ in this case.

5.2 Clustering in Rubber-Toughened PVC

Figure 9 shows a series of scanning electron microscope (SEM) photographs of the fracture surface of a rubber-toughened polyvinyl chloride (PVC) specimen. Note that large voids on the surface contain smaller voids, which contain still smaller voids, and so on. In addition, the photographs at different magnifications look similar, though not identical, indicating a nearly self-similar void structure.

Such a void structure could be produced by fractal clustering of rubber particles, such as the idealized arrangement in Fig. 3. Microvoids that form at the rubber particles could link other voids in the immediate vicinity, forming a larger void. These larger voids could then link with other voids formed from particle clusters, and so on. This type of particle distribution might be one source of the enhanced toughness in rubber-toughened polymers.

We evaluated the fracture surface at the various magnifications with image analysis. Figure 10 is a log-log plot of void density (number of voids/projected area of fracture surface) versus void diameter for two samples of PVC. The curves are fairly linear for both samples over roughly two decades, and $D \approx 1.4$ for the void distribution.

The fractal model on void and particle distribution has upper and lower limits on validity, however. The minimum void size corresponds the particle diameter, and the upper limit on void size is on the order of the surface roughness, which is an order of magnitude smaller than the sample cross section.

5.3 Mode II Delamination of Graphite/Epoxy Laminates

When a graphite/epoxy laminate specimen with a pre-existing delamination is subject to Mode II loading, an array of microcracks forms in front of the macroscopic crack. We performed Mode II delamination experiments on such a composite material in an effort to determine if the resulting microcrack distribution is fractal

We loaded subsize split laminate specimens in three-point bending using a tensile stage mounted inside an SEM. These in situ tests enable real-time observation of damage [17]. The material was an AS4/3502 composite, which was chosen because previous studies indicated that this material produces an extensive damage zone.

Figure 11 is a series of SEM photographs which show the stages of development of a crack tip damage zone. Microcracks form in the resin-rich zone between plies; the microcracks are oriented 45° from the macroscopic plane, such that the maximum local tensile stress is normal to the microcracks. Upon further deformation, the microcracks coalesce with the main crack tip, resulting in macroscopic crack growth.

Note that the size and spacing of the microcracks in Fig. 11 is relatively uniform. *The microcrack distribution is not fractal in this case*; rather, it apparently is governed by the boundary conditions in the body. The Mode II loading of the specimen induces significant tensile stresses in the resin, which contains an initial distribution of flaws (that may be fractal). One of these flaws becomes unstable and propagates normal to the maximum tensile stress; it arrests when it reaches the fiber-rich zones on either side. When a second microcrack initiates further ahead of the macroscopic crack tip, a small volume of material is isolated between the microcracks; this material is shielded from further stressing; subsequent cracking in this region is therefore unlikely. This process is repeated, as the damage zone forms and the macroscopic crack grows by coalescing with the trailing edge of the damage zone. The microcrack spacing is governed by a competition between a decaying stress field away from the tip of the damage zone and the need to sample sufficient material to find a critical nucleus for microcrack initiation.

In summary, this experimental study indicated that the damage zone that forms ahead of a macrocrack subject to Mode II loading is not fractal, but the initial flaw distribution resulting from fabrication may be fractal. We have attempted to model the damage zone with finite element analysis in order to evaluate local stress fields, but we have yet to obtain satisfactory results.

6.0 SUMMARY AND CONCLUSIONS

Fractal geometry can describe microstructural heterogeneity simply and compactly. Both the size distribution and spatial distribution can be characterized with a fractal dimension. The scaling nature of fractals may prove to be useful when formulating models to connect microscale damage with global mechanical response.

This study represents a preliminary investigation of the usefulness of fractal geometry in damage modeling. One of the most important results was the derivation of the Weibull distribution for the strength of brittle solids, where a relationship between the Weibull shape parameter and the fractal dimension of the flaw distribution was demonstrated. Previously, the Weibull distribution was merely a phenomenological description fracture strength. This research also resulted in simple models for stable damage development, which indicate that the recent work by Schapery [14] on path-independent work potentials may provide a framework for developing refined damage models for materials with fractal microstructures.

Several examples of fractal phenomena in real materials were presented, including the flaw size distribution in glass and the particle spatial distribution in rubber-toughened PVC. Mode II loading of a split laminate graphite/epoxy specimen produces an array of microcracks, but the distribution is not fractal for the material studied. However, these microcracks initiate from a distribution of initial flaws that may be fractal. It appears that fractal microstructures can form when there is some degree of randomness; for example, the flaw size distribution in glass and the particle distribution in the polymer specimens were the result of material processing. Fractal structures are much less likely when the features form as a result of deterministic rules, such as the microcrack propagation and arrest in the composite specimen.

The recommended areas for further study include:

- Application of the path independent potential approach or other methodology to develop three-dimensional damage evolution models for materials with fractal microstructures. The ultimate goal would be a unified model to relate microstructure to global mechanical response.

- Development of void growth models that quantify the relationship between fractal clustering and toughening.
- Incorporation of related mathematical concepts such as percolation theory and chaos theory into damage models.
- Further analysis of damage zone development during Mode II delamination of fiber-reinforce composites.

7.0 REFERENCES

1. Evans, A.G., "The New High Toughness Ceramics." ASTM STP 907, American Society for Testing and Materials, Philadelphia, 1989, pp. 267-291.
2. Mandelbrot, B.B., *The Fractal Geometry of Nature*, W.H. Freeman and Company, New York, 1982.
3. Haritos, G.K., Hager, J.W., Amos, A.K., Salkind, M.J., and Wang, A.S.D., "Mesomechanics: the Microstructure-Mechanics Connection." *International Journal of Solids and Structures*, Vol. 24, 1988, pp. 1081-1096.
4. Hurd, A.J., Weitz, D.A., and Mandelbrot, B.B., eds., *Proceedings of the First Symposium on Fractal Aspects of Materials: Disordered Systems*, Materials Research Society, Pittsburgh, 1987.
5. Weitz, D.A., Sander, L.M., and Mandelbrot, B.B., eds., *Proceedings of the Second Symposium on Fractal Aspects of Materials: Disordered Systems*, Materials Research Society, Pittsburgh, 1988
6. Kaufman, J.H., Martin, J.E., and Schmidt, P.W., eds., *Proceedings of the Third Symposium on Fractal Aspects of Materials: Disordered Systems*, Materials Research Society, Pittsburgh, 1989.

7. Mandelbrot, B.B., Passoja, D.E., and Paullay, A.J., *Nature*, Vol. 300, 1984, pp. 721-722.
8. Louis, E. and Guinea, F., "The Fractal Nature of Fracture." *Europhysics Letters*, Vol. 3, 1987, pp. 871-877.
9. Rosenfield, A., "Fractal Mechanics." *Scripta Metallurgica*, Vol. 21, 1987, pp. 1359-1363.
10. Passoja, D.E., "Fundamental Relationships between Energy and Geometry in Fracture." *Advances in Ceramics*, Vol. 22, 1988, pp. 101-126.
11. Weibull, W., "A Statistical Distribution Function of Wide Applicability." *Journal of Applied Mechanics* Vol. 18, 1953, pp. 293-297.
12. Weiderhorn, S.M. and Fuller, E.R., "Structural Reliability of Ceramic Materials." *Materials Science and Engineering*, Vol. 71, 1985, pp. 169-186.
13. Wagner, H.D., Phoenix, S.L., and Schwartz, P., "A Study of Statistical Variability in the Strength of Single Aramid Filaments." *Journal of Composite Materials*, Vol. 18, 1984, pp. 313-338.
14. Schapery, R.A., "A Theory of Mechanical Behavior of Elastic Media with Growing Damage and Other Changes in Structure." *Journal of the Mechanics and Physics of Solids*, Vol 38, pp. 215-253.
15. Griffith, A.A. "The Phenomena of Rupture and Flow in Solids." *Philosophical Transactions, Series A*, Vol. 221, 1920, pp. 163-198.
16. Anderegg, F.O., "Strength of Glass Fibers." *Ind. Eng. Chem.*, Vol. 31, 1939, pp. 290-298.
17. Hibbs, M.F., Tse, M.K., and Bradley, W.L., "Interlaminar Fracture Toughness and Real-Time Fracture Mechanism of Some Toughened Graphite/Epoxy Composites." ASTM STP 937, American Society for Testing and Materials, Philadelphia, 1987, pp. 115-130.

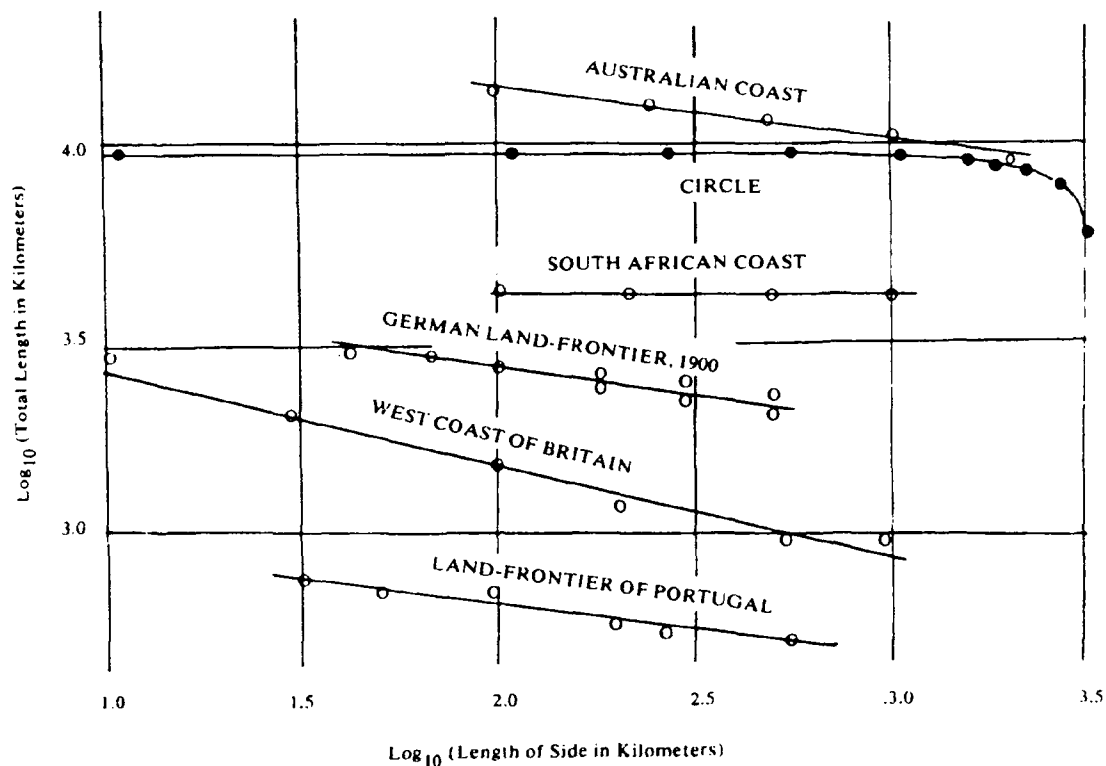


FIGURE 1. Coastline length measurements as a function of the length of the line segment used to approximate the coastline [2]. When a Euclidian shape such as circle is approximated by a series of line segments, the perimeter converges to the true value as the size of the segment decreases. When a curve is fractal, however, the true length is infinite, and the measured length does not converge.

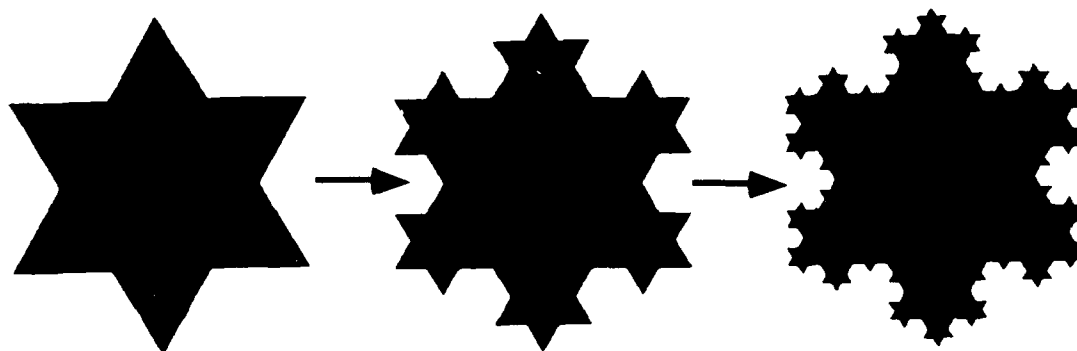


FIGURE 2. Koch snowflake [2], which is generated by adding two small apexes to each larger apex; this construction is carried on to infinity, such that the resulting shape has an infinite perimeter but a finite area. $D = \log 4 / \log 3 = 1.2618$ in this case.

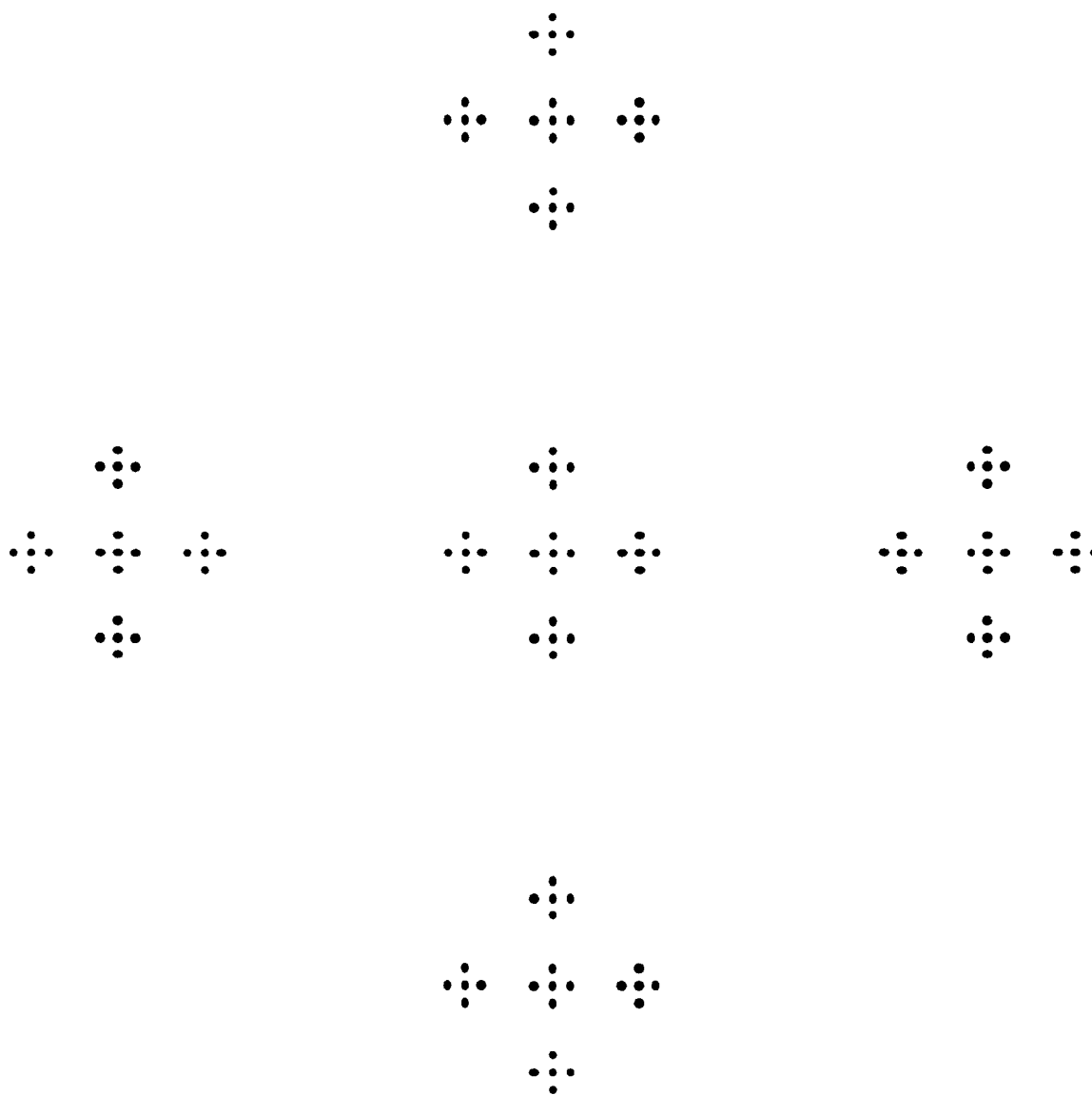


FIGURE 3. Example of self-similar fractal clustering in two dimensions. $D = 1$ for this arrangement.

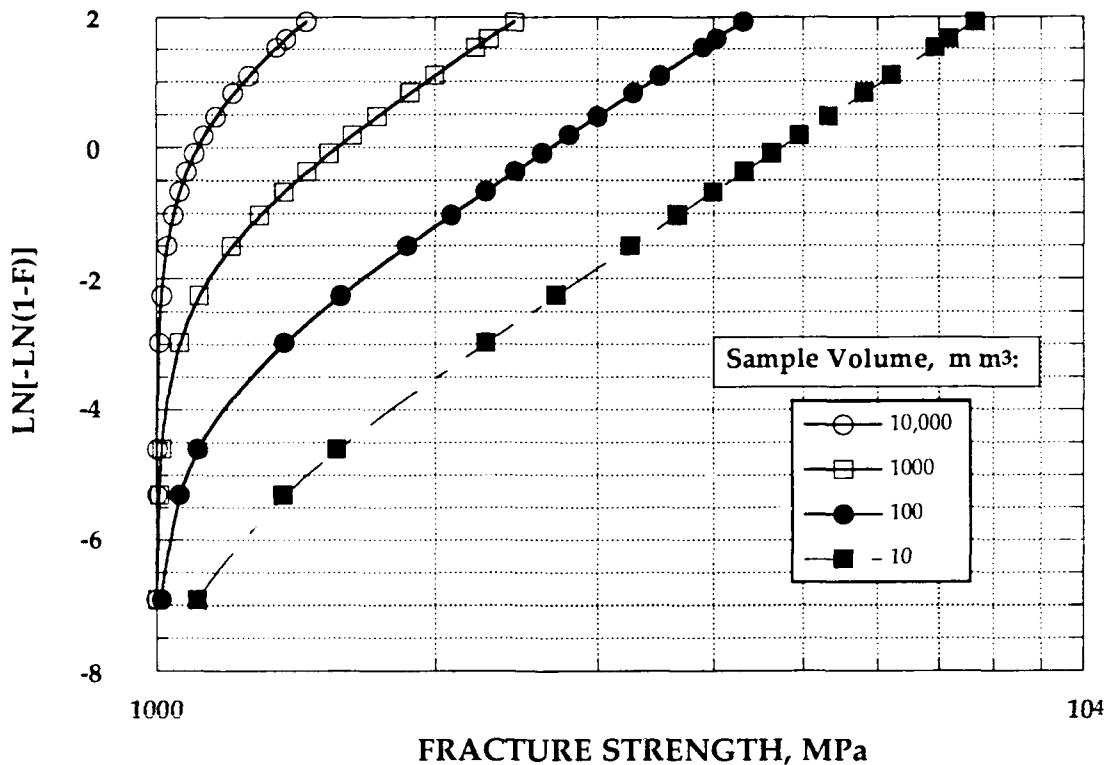


FIGURE 4. Two-parameter Weibull plot of Eq. (11).

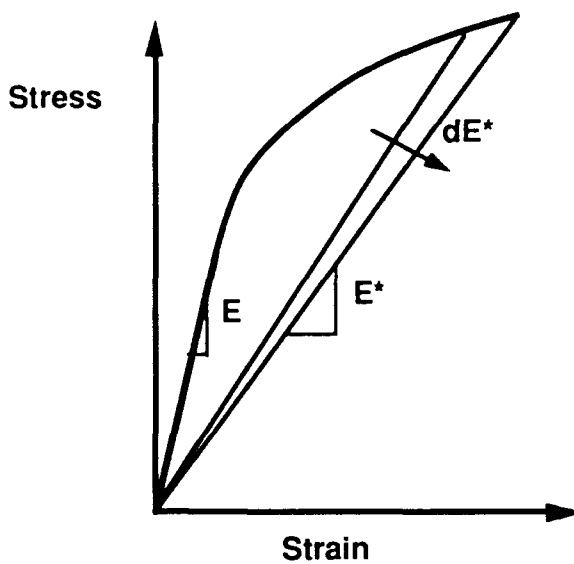


FIGURE 5. Schematic stress-strain curve, as predicted by Eq. (19).

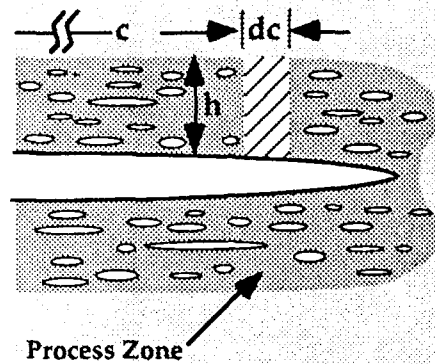


FIGURE 6. Process zone created during propagation of a macroscopic crack.

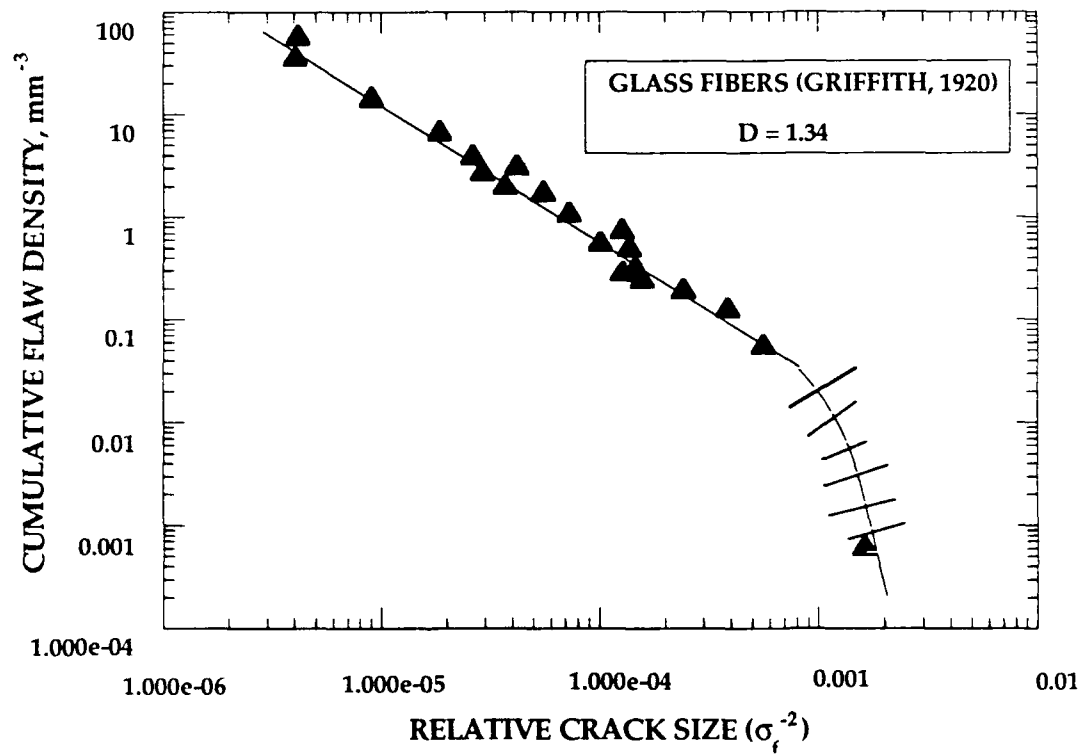


FIGURE 7. Fracture strength data for glass fibers from Griffith [15], which shows that the flaw size distribution is fractal over several orders of magnitude.

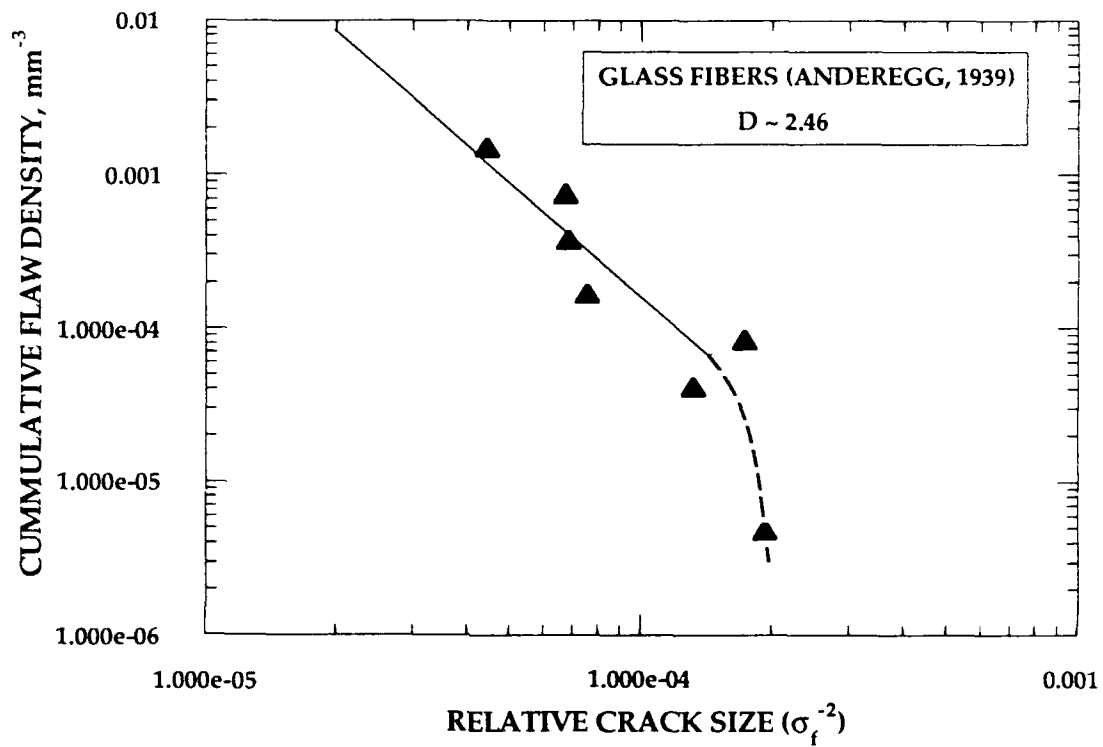


FIGURE 8. Strength data for glass fibers from Anderegg [16].

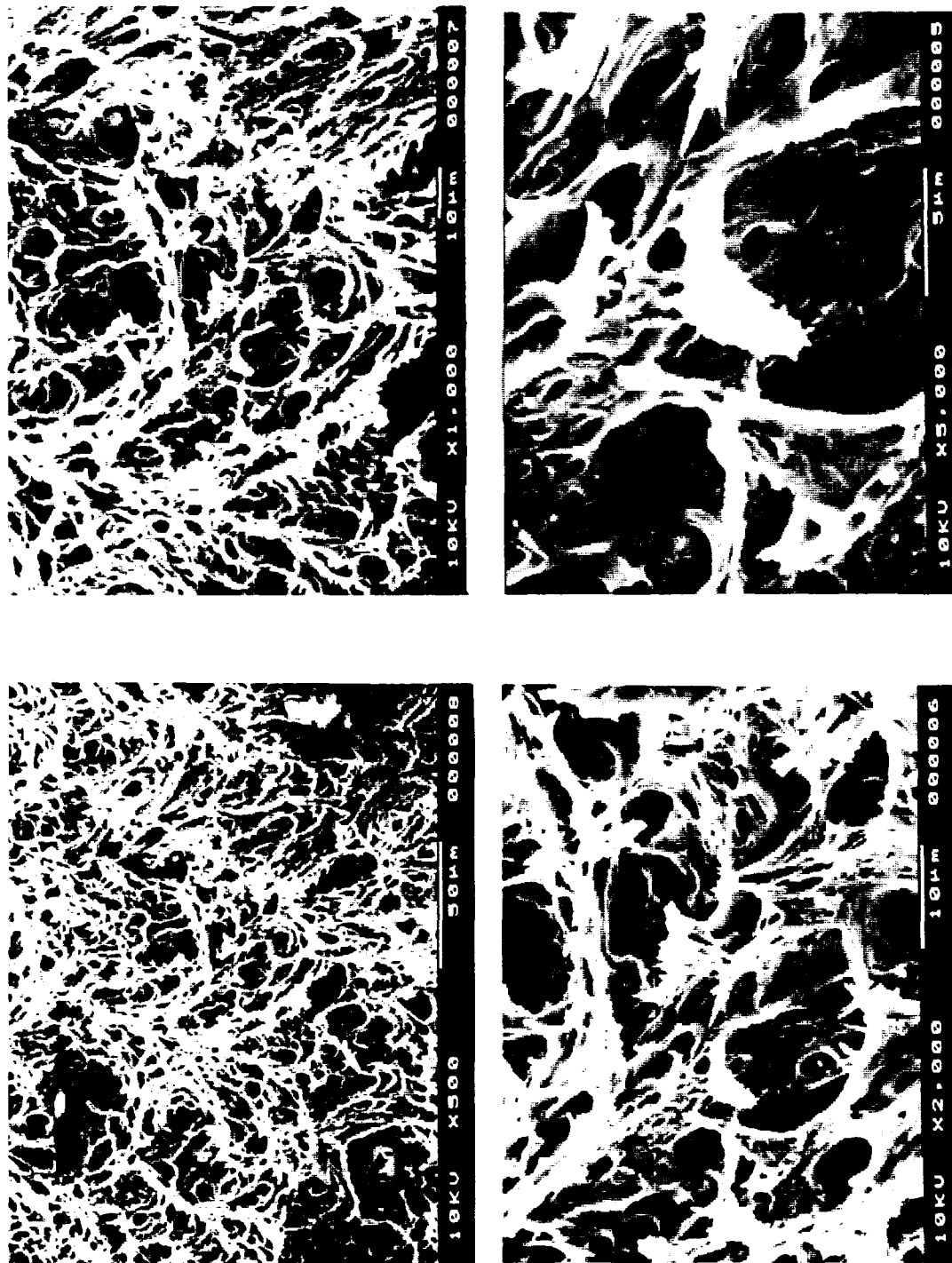


FIGURE 9 Fracture surfaces in rubber-toughened polycarbonate which exhibit a microvoid structure that is approximately self similar. Photographs have been reduced to 80% or their original size.

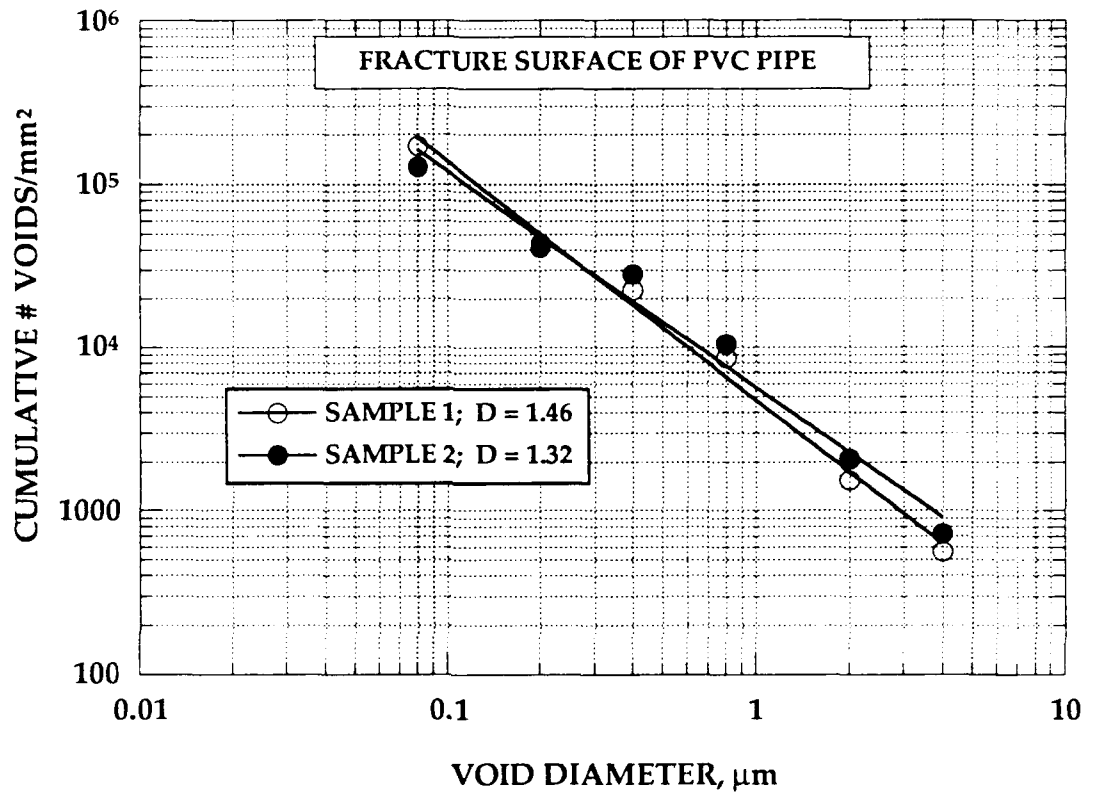


FIGURE 10. Void density versus void diameter for rubber-toughened PVC.



FIGURE 11. Sequence of SEM photographs that show the development of a damage zone during a Mode II delamination test.